THE JOURNAL OF PHYSICAL CHEMISTRY B

Article

Cite This: J. Phys. Chem. B 2018, 122, 11206−11217

pubs.acs.org/JPCB

Measuring Solvent Hydrogen Exchange Rates by Multifrequency Excitation ^{15}N CEST: Application to Protein Phase Separation

Tairan Yuwen,[†] Alaji Bah,[‖,▽] Jacob P. Brady,[†] Fabien Ferrage,[⊥] Guillaume Bouvignies,[⊥] and Lewis E. Kay*[,†,‖]

[†]Departments of Molecular Genetics, Biochemistry and Chemistry, University of Toronto, Toronto, Ontario M5S 1A8, Canada

[‖]Hospital for Sick Children, Program in Molecular Medicine, 555 University Avenue, Toronto, Ontario M5G 1X8, Canada

[⊥]Laboratoire des Biomolécules, LBM, Département de Chimie, École Normale Supérieure, PSL University, Sorbonne Université, CNRS, 75005 Paris, France

Supporting Information

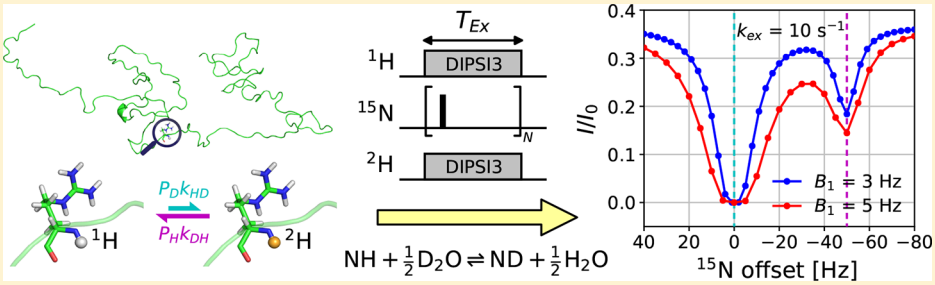

ABSTRACT: Solvent exchange rates provide important information about the structural and dynamical properties of biomolecules. A large number of NMR experiments have been developed to measure such rates in proteins, the great majority of which quantify the buildup of signals from backbone amides after initial perturbation of water magnetization. Here we present a different approach that circumvents the main limitations that result from these classical hydrogen exchange NMR experiments. Building on recent developments that enable rapid recording of chemical exchange saturation transfer (CEST) pseudo-3D data sets, we describe a ^{15}N-based CEST scheme for measurement of solvent exchange in proteins that exploits the one-bond ^{15}N deuterium isotope shift. The utility of the approach is verified with an application to a 236 residue intrinsically disordered protein domain under conditions where it phase separates and a second application involving a mutated form of the domain that does not phase separate, establishing very similar hydrogen exchange rates for both samples. The methodology is well suited for studies of hydrogen exchange in any ^{15}N-labeled biomolecule. A discussion of the merits of the CEST experiment in relation to the popular CLEANEX-PM scheme is presented.

INTRODUCTION

The pioneering hydrogen exchange experiment established by Linderstrøm-Lang in the 1950s has played an important role in defining the field of protein science and in establishing the notion that proteins are dynamic molecules.[1,2] In the intervening 70 years that have passed it has become clear that protein motions can be fundamental to both function and misfunction[3−6] and, building on the initial methodology developed by Linderstrøm-Lang and his laboratory, hydrogen exchange experiments continue to play a role in expanding our understanding of structure−dynamics−function relationships in biomolecules.[7−11] An important technology in this regard has been nuclear magnetic resonance (NMR) spectroscopy because residue-specific hydrogen exchange rates can be measured over a broad spectrum of time-scales.[12] Slow exchange processes (exchange lifetimes on the order of several hundreds of seconds) can be quantified by monitoring the disappearance of site-specific NMR signals as a function of time after addition of D_2O to a lyophilized protein sample.[1,13,14] Faster processes (lifetimes ∼10 ms to 1 s), in turn, are most often studied by perturbing the water resonance and quantifying the changes in intensities of amide signals over time that arise from the initial perturbation.[15−21] Extraction of accurate exchange rates is complicated, however, by the fact that the network of protons in a protein is highly coupled and extensive so that hydrogen exchange must be separated from magnetization exchange that derives from ^{1}H−^{1}H cross-relaxation in the molecule. This has led to the development of a second class of experiment that relies on deuterium isotope shifts of probe spins in which samples are prepared with both H_2O and D_2O solvent, typically in ratios close to 1:1.[22,23] By separating peaks according to whether they report on deuterated or protonated amides and quantifying conversion from N−D to N−H or *vice versa*, hydrogen exchange

Special Issue: William A. Eaton Festschrift

Received: July 16, 2018
Revised: August 31, 2018
Published: September 4, 2018

DOI: 10.1021/acs.jpcb.8b06820
J. Phys. Chem. B 2018, 122, 11206−11217

rates can be extracted without some of the complications that are associated with experiments that are based on selective perturbation of the water resonance. However, there is a trade-off with sensitivity, as this second type of measurement involves triple-resonance-based pulse schemes with relatively long transfer delays. Finally, very rapid exchange processes (many thousands s^{-1}) can be studied indirectly using triple resonance experiments that monitor the decay of ^{15}N transverse magnetization when multiple chemical shift refocusing pulses are applied with and without ^{1}H decoupling.[24,25]

Like Linderstrøm-Lang's hydrogen exchange approach, the Forsén and Hoffman chemical exchange saturation transfer (CEST) experiment[26] was developed many decades ago. In perhaps its most important use, CEST has played a leading role in MRI imaging by exploiting differences in solvent hydrogen exchange properties between diseased and surrounding healthy tissues leading to enhanced contrast and hence detailed images of areas of pathology.[27,28] Notably, CEST can also be used to study biomolecular dynamics involving chemical exchange processes that derive from the interconversion of two or more conformers, even in cases where the spectrum of only one of the conformers (ground state) is observed.[29,30] The sensitivity of the CEST approach to hydrogen exchange processes that are exploited in MRI and to exchange between distinct conformers that are studied in biomolecular applications suggests that it should be possible to develop the CEST technique for studies of site-specific hydrogen exchange in biomolecules. However, as we describe below this experiment had to await the significant acceleration of CEST data collection exploiting multisite excitation schemes,[31−33] that, in turn, enables the use of very weak effective radio frequency (RF) fields that are necessary for measuring small exchange rates (<50 s^{-1}), as would typically be expected for hydrogen exchange at most backbone amide sites in a protein under physiological conditions. With these developments now in place, we present here such a CEST scheme. We first show that accurate exchange rates and populations of rare protein states can be obtained using ^{15}N-CEST with weak B_1 fields of 5 Hz or less, which are required in hydrogen exchange studies. Subsequently, we illustrate the utility of the CEST method with hydrogen exchange applications to an intrinsically disordered domain from the Ddx4 protein[34,35] in which all Arg residues are substituted by Lys, $Ddx4_{RtoK}$, that does not phase separate, and to a second sample, $Ddx4_{cond}$, that phase separates under the conditions of our study. Accurate hydrogen exchange rates are extracted from both Ddx4 samples. The advantages of the present approach over other methodologies are also described.

METHODS

Sample Preparation. An NMR sample of a 2 mM [U−^{15}N]-labeled A39G FF domain (50 mM sodium acetate pH 5.7, 100 mM NaCl, and ∼90% H_2O/∼10% D_2O) was prepared as described previously.[29,36] Human $Ddx4_{1-236}$ (referred to in what follows as $Ddx4_{cond}$) and a mutant that does not phase separate, where all Arg residues were replaced by Lys, $Ddx4_{RtoK}$, were expressed and purified as described in the literature.[34,35] The phase-separated Ddx4 sample comprises ∼400 mg/mL protein of which ∼10% is [U−^{15}N]-labeled, while the concentration of $Ddx4_{RtoK}$ is 2 mM in [U−^{15}N]-labeled protein. Both samples were prepared in NMR buffer containing 20 mM sodium phosphate (pH 6.5), 100 mM NaCl, 5 mM TCEP, 0.02% NaN_3, and ∼90% H_2O/∼10% D_2O. In $Ddx4_{cond}$ all Cys residues were replaced with Ser to minimize the potential for oxidation.

NMR Spectroscopy. All NMR experiments were performed on an 800 MHz AVANCE III Bruker spectrometer equipped with a cryogenically cooled probe with a *z*-axis pulsed field gradient coil. The field strength for the DANTE pulses, applied during D-CEST elements, $B_1^{\text{D-CEST}}$, was set 6 dB lower than the maximum (∼3.5 kHz), generating an effective CEST field strength of $\frac{\tau_p}{\tau'}B_1^{\text{D-CEST}}$, where τ_p is the DANTE pulse width and τ' the duration between successive DANTE pulses.[31] As described previously,[31] τ' is set from the relation, $sw_{CEST} = \frac{1}{\tau'}$, where sw_{CEST} is the region that is swept by the weak B_1 field (1 frequency at a time in successive 2D planes) and τ_p subsequently adjusted accordingly to give the desired effective field strength.

^{15}N D-CEST experiments for A39G FF (1 °C) were carried out using effective DANTE B_1 fields of 3 Hz (τ_p = 4.8 μs), 5 Hz (τ_p = 6.0 μs), 10 Hz (τ_p = 4.5 μs), and 20 Hz (τ_p = 7.1 μs), with the position of RF field varied over 180, 240, 640, and 800 Hz (sw_{CEST}), respectively, using step-sizes of 3, 5, 10, and 20 Hz. This sample was used to verify the methodology prior to applications involving hydrogen exchange. Pseudo-3D CEST data sets containing 62 (B_1 = 3 Hz), 50 (B_1 = 5 Hz), 66 (B_1 = 10 Hz), and 42 (B_1 = 20 Hz) 2D planes were generated. The D-CEST period, T_{Ex}, was set to 1 s; each 2D plane was recorded with two transients per FID. The prescan delay was 2.5 s, and (768, 64) complex points in (t_2, t_1) were recorded, to give a net acquisition time of ∼15 min per spectrum. Measurement times for D-CEST experiments with B_1 fields of 3, 5, 10, and 20 Hz were ∼16, ∼13, ∼17, and ∼11 h, respectively.

^{15}N D-CEST experiments were recorded on $Ddx4_{cond}$ and $Ddx4_{RtoK}$ (30 °C) using effective B_1 DANTE fields of 3 Hz (τ_p = 7.1 μs), 5 Hz (τ_p = 9.5 μs), and 8 Hz (τ_p = 14.3 μs) with sw_{CEST} set to 120, 150, and 160 Hz, respectively. Note that the choices of sw_{CEST} in these applications are based mainly on the spacing between major and minor dips in CEST profiles, which, in the case of applications involving solvent hydrogen exchange, is given by the one-bond ^{2}H isotope shift for amide nitrogens, $^{1}\Delta^{15}N(D)$, taking into account the fact that the dip line width increases with the strength of the B_1 field.[37] In this manner, overlap between the major and minor dips is avoided. The position of the RF field carrier was shifted by 3 (sw_{CEST} = 120 Hz), 5 (sw_{CEST} = 150 Hz), and 8 (sw_{CEST} = 160 Hz) Hz in each 2D data set, generating pseudo-3D CEST data sets containing 42, 32 and 22 2D planes, respectively. T_{Ex} = 1 s, and each 2D plane was recorded with two transients per FID. The prescan delay was 2.5 s with (768, 128) complex points in (t_2, t_1) to give a net acquisition time of ∼30 min/spectrum. Measurement times for D-CEST experiments with effective B_1 fields of 3, 5, and 8 Hz were ∼21, ∼16, and ∼11 h, respectively.

Each of the pseudo-3D data sets was recorded with a reference plane where the D-CEST relaxation period, T_{Ex}, was omitted, so as to obtain robust estimates of longitudinal relaxation rates.[29] Calibration of the weak (effective) ^{15}N B_1 field strengths followed the approach of Guenneugues et al.[38] with a modified scheme to achieve accurate results in cases of very weak B_1 fields, as described in the text.

CLEANEX-PM experiments were carried out on $Ddx4_{cond}$ and $Ddx4_{RtoK}$ samples (30 °C), following the previously described pulse sequence.[20] A 7.5 ms REBURP pulse[39] was applied to selectively perturb water magnetization at the start of the scheme, with very similar results obtained using a Gaussian shaped selective pulse instead. Each 2D data set was recorded

DOI: 10.1021/acs.jpcb.8b06820
J. Phys. Chem. B 2018, 122, 11206−11217

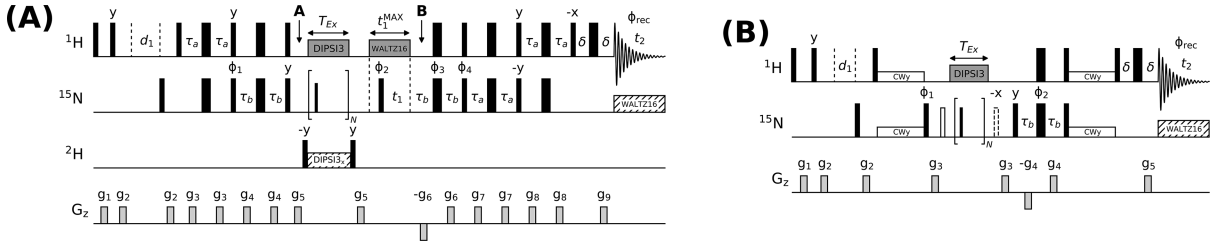

Figure 1. (A) ^{15}N D-CEST pulse scheme for the measurement of solvent hydrogen exchange rates. All ^{1}H and ^{15}N 90° (180°) RF pulses are shown as narrow (wide) rectangles and are applied at the highest possible power levels. The DANTE ^{15}N pulses during T_{Ex} are set 6 dB lower than the highest possible power level (although higher power levels can be applied[31]). ^{1}H decoupling during T_{Ex} and during t_1 is achieved with ∼4 kHz DIPSI-3[52] and WALTZ-16[56] elements, respectively. WALTZ-16 decoupling is applied for a total duration of t_1^{MAX} so that the amount of heating is independent of t_1. ^{15}N decoupling during acquisition is achieved with WALTZ-16 (1.3 kHz); a 500 Hz DIPSI-3 ^{2}H decoupling field is applied during T_{Ex}. The ^{1}H carrier is initially placed on the water signal, moved to the middle of the amide region immediately before the T_{Ex} period, and subsequently returned to the water frequency after t_1 (indicated by the region between arrows labeled with A and B). The ^{15}N carrier is placed in the center of the amide region and shifted to the desired offset during the ^{15}N D-CEST period. For the reference plane where $T_{Ex} = 0$, the ^{1}H DIPSI-3 element is applied for a duration of T_{Ex} immediately after acquisition to ensure equal heating in all planes. All pulse phases are assumed to be x, unless otherwise indicated. The phase cycle is $\phi_1 = x, -x$; $\phi_2 = y$; $\phi_3 = 2(x), 2(y), 2(-x), 2(-y)$; $\phi_4 = x$; $\phi_{rec} = x, -x, -x, x$; with a minimum phase cycle of 2. The delays are $\tau_a = 2.38$ ms, $\tau_b = 1/(4|^1J_{HN}|) = 2.68$ ms, $\delta = 500$ μs. Gradients are applied with the following durations (ms) and strengths (in % maximum of ∼60 G/cm): g_1 (1.0, 10%), g_2 (1.0, 20%), g_3 (0.5, 12%), g_4 (0.5, 24%), g_5 (1.0, −75%), g_6 (0.625, 80%), g_7 (0.5, 60%), g_8 (0.5, 15%), g_9 (0.256, 39.6%). Gradients g_6 and g_9 are used for coherence selection and should be optimized for maximum signal. Quadrature detection in the indirect dimension is obtained using the gradient-based enhanced sensitivity approach[57,58] by recording two sets of spectra with (ϕ_4, g_9) and ($\phi_4 + \pi$, $-g_9$) for each t_1 increment. The phase ϕ_2 is incremented along with the phase of the receiver by 180° for each complex t_1 point.[59] (B) Pulse scheme for calibration of the very weak CEST B_1 field. Many of the details are as for panel A and are not repeated. In this approach calibration is achieved by selecting a peak of interest using a double heteronuclear cross-polarization element with ∼40 Hz B_1 fields applied on both channels for a duration of $1/(|^1J_{HN}|) = 10.8$ ms.[60,61] During this period RF carriers for both ^{1}H and ^{15}N are placed on resonance with the peak that is used for B_1 calibration. The power level of DANTE pulses during T_{Ex} is set to the value used in ^{15}N D-CEST. Quadrature is obtained by recording a pair of spectra, with and without the dashed ^{15}N pulse (phase $-x$) for each T_{Ex} value. Note that when the two ^{15}N 90° pulses flanking the T_{Ex} period (open pulses) are omitted a pair of peaks is obtained, separated by twice the B_1 field; this is the "typical" setup for calibration of fields on the order of 10 Hz or greater. The phase cycle is $\phi_1 = x, -x$; $\phi_2 = 2(x), 2(y), 2(-x), 2(-y)$; $\phi_{rec} = x, -x, -x, x$; with a minimum phase cycle of 2. The delays are $\tau_b = 1/(4|^1J_{HN}|) = 2.68$ ms, $\delta = 500$ μs. Gradients are applied with the following durations (ms) and strengths (in % maximum): g_1 (1.0, 10%), g_2 (1.0, 20%), g_3 (1.0, −75%), g_4 (0.625, 80%), g_5 (0.256, 39.6%). Gradients g_4 and g_5 are used for coherence selection and should be optimized for maximum signal.

with 4 transients/FID, a relaxation delay of 2 s, and (768, 128) complex points in (t_2, t_1) to give a net acquisition time of ∼35 min/spectrum. Ten different τ_{mix} values in the range 10−100 ms were chosen in order to measure the amide $^{1}H^{N}$ magnetization buildup curve. A separate reference 2D plane was recorded with 2 transients/FID and a relaxation delay of 15 s to estimate the equilibrium magnetization at each site. The total measurement time for all the experiments was ∼8 h. The apparent relaxation rate of water magnetization during the CLEANEX-PM element was measured as described in Supporting Information.

Data Analysis. NMR spectra were processed and analyzed using the *NMRPipe* suite of programs,[40] with peak intensities extracted with the *autofit* subroutine. D-CEST profiles were analyzed with the software package *ChemEx*,[41] using a separate module for fitting ^{15}N D-CEST data sets that is available from the authors upon request. Fits of ^{15}N D-CEST profiles were performed in a manner similar to the analysis of regular ^{15}N CEST data sets[29] with the exception that the population of the excited state (*i.e.*, population of N−D spin pairs for a given amide in the case of hydrogen exchange), p_E, was taken as a global parameter (see text), with solvent hydrogen exchange rates, k_{ex}, fit on a per-residue basis. Differences in ^{15}N longitudinal relaxation rates for ^{15}N−^{1}H and ^{15}N−D spin pairs have been taken into account by assuming that $R_{1,N_D} \approx \eta R_{1,N_H}$, with $\eta = 0.50$ at 800 MHz, as described in the text. Fitting of CLEANEX-PM data sets followed the procedure described in the literature;[20] a number of additional details are provided in Supporting Information.

RESULTS AND DISCUSSION

Multifrequency CEST Excitation Schemes Are Essential for Recording Hydrogen Exchange CEST Data Sets. A typical protein CEST experiment is recorded as a series of 2D data sets, with the position of the weak, continuous wave (CW) B_1 field varied by approximately B_1 Hz between each 2D spectrum, "in search" of invisible excited states.[42] When the B_1 field is proximal to the resonance position of a spin in the excited state, the perturbation that ensues is transferred to the ground state peak by chemical exchange, leading to a decrease in its intensity; a larger decrease in intensity is observed when the field is placed proximal to the corresponding resonance in the ground state. By measuring the intensity of the peak from the ground conformer as a function of the B_1 position, a CEST profile is generated, from which the positions of major and minor state resonances as well as exchange rates and fractional populations of exchanging states are obtained by quantifying the dips in the profile. As the line widths of the CEST dips depend on the strength of the applied weak B_1 field,[42] scaling with B_1 in the limit that $2\pi B_1 \gg k_{ex}$[37] (see eq 18 of ref 37 for the exact relationship), it is important that weak fields be used in cases where chemical shift differences are small. Further, it is important to choose B_1 field strengths judiciously, with at least one of the fields in a set of recorded CEST experiments on the order of k_{ex}.[42] Note that, for $2\pi B_1 \gg k_{ex}$, corresponding to the slow exchange limit in CEST, populations and exchange rates cannot be separated.

Our goal here is to exploit the one-bond ^{2}H isotope shift of amide ^{15}N spins, $^{1}\Delta^{15}N(D)$, to measure solvent exchange. In the applications that we consider, where samples are prepared with a solvent composition of $P_H(H_2O)/P_D(D_2O)$ and $P_H(P_D = 1 - P_H)$ is the fractional amount of $H_2O(D_2O)$ in the buffer

DOI: 10.1021/acs.jpcb.8b06820
J. Phys. Chem. B 2018, 122, 11206−11217

(typically $P_H \sim 90\%$), we can write the solvent exchange reaction at a backbone amide site as[43]

$$NH + \frac{1}{2}D_2O \underset{k_{DH}}{\overset{k_{HD}}{\rightleftarrows}} ND + \frac{1}{2}H_2O \quad (1)$$

By analogy to a "typical" two-site exchange process, the fractional populations of the ground (visible, NH) and excited (invisible, ND) states are given by p_G and p_E, respectively, with a chemical shift difference $\Delta\varpi_{GE} = \varpi_E - \varpi_G = {}^1\Delta^{15}N(D) \sim -0.7$ ppm.[22] As the $\Delta\varpi_{GE}$ values are small, it is necessary to apply weak B_1 fields (<10 Hz) to resolve the minor and major state dips in the CEST profile (see below). Further, the optimal choice of the B_1 field for the accurate determination of exchange parameters (p_E, k_{ex}) is also governed by k_{ex},[42] with B_1 values less than ~5 Hz required for studying solvent exchange processes with $k_{ex} \sim 10\ s^{-1}$ (so that p_E and k_{ex} can be separated, see above). This requirement challenges the recording of conventional CEST data sets using a CW field that would be spaced in increments of ~5 Hz that are required to properly define each of the dips since for a typical ^{15}N spectral width of 25 ppm and a static magnetic field strength of 18.8 T (800 MHz ^1H frequency) 400 2D data sets would be required. The development of rapid modes for CEST acquisition has thus been critical.[31−33] One approach that we exploit here uses a recently described DANTE[44,45] multiple excitation scheme (D-CEST) in which short pulses of duration τ_p and strength $B_1^{D\text{-}CEST}$ are applied at intervals separated in time by τ'.[31] The resulting excitation profile is equivalent to that obtained by applying a series of CW pulses of strength $\frac{\tau_p}{\tau'}B_1^{D\text{-}CEST}$ separated in frequency by $sw_{CEST} = \frac{1}{\tau'}$. Thus, by using this approach, the carrier frequency of the B_1 field is swept over a range corresponding to sw_{CEST} that can be much less than sw to obtain complete coverage of the spectral width of interest (sw), leading to large savings in measurement times (by $sw/sw_{CEST} > 10$ in the present set of applications).

Experimental and Practical Considerations. Figure 1A shows the ^{15}N D-CEST pulse scheme that has been developed for the hydrogen exchange applications considered here. The sequence follows very closely other ^{15}N CEST experiments,[29] and only a number of important differences are highlighted here. Unlike previous applications of CEST that monitored exchange between conformers probed using protonated amide groups,[29,46−48] in the present study exchange involves an interchange between NH and ND moieties (eq 1). As described previously,[49] scalar relaxation of the second kind[50] can significantly broaden ^{15}N signals derived from deuterated amides, giving rise to broad minor state dips in CEST profiles and hence decreased sensitivity. A 500 Hz ^2H decoupling field is applied throughout the course of the CEST element that significantly sharpens the ND dips. Concomitantly, ^1H decoupling is also utilized, collapsing doublet components that would otherwise appear in major dips of CEST profiles arising from one-bond $^{15}N-^1H$ scalar couplings. We have previously shown that the ^1H decoupling scheme must be chosen carefully to avoid sidebands that then become amplified via CEST and recommended the use of a $90_x240_y90_x$[51] sequence that achieves decoupling over a bandwidth covering all amide protons in protein applications, with a short repetition cycle that "pushes" the sidebands beyond the expected region where "real" peaks would appear.[29] However, this decoupling sequence is not sufficiently broadbanded to extend to aliphatic protons. For most studies, this is irrelevant as CEST B_1 fields are significantly larger than the residual small multibond $^{15}N-^1H$ couplings that persist, and line widths are typically dominated by the B_1 field strength. In the present applications, however, very weak ^{15}N B_1 fields are used (see below) so that these small couplings could result in broadening of the CEST dips and thus could modify their intensities. We have therefore used a DIPSI-3 scheme[52] that decouples over a wider bandwidth than the $90_x240_y90_x$[51] sequence so as to eliminate evolution from $^2J_{HN}$ (2−3 Hz[53]) and $^3J_{HN}$ (2−3 Hz[54]) couplings. Simulations show that this scheme suppresses the $^1J_{HN}$ coupling, as expected, but also the effects of couplings at least as large as 5 Hz that derive from a proton located −4 kHz from the ^1H carrier (such as an H^α), as illustrated in Figure S1. Simulations (Figure S2) and experiment further establish that sidebands are not observed in CEST profiles using DIPSI-3 so long as B_1 fields <10 Hz are employed. Finally, because applications are focused on intrinsically disordered proteins (the Ddx4 fragment we use is 236 residues) where resolution is critical, we have opted to record ^{15}N chemical shift evolution in a mode where magnetization is in-phase using ^1H decoupling.[55]

Simulations establish that careful calibration of the weak B_1 field is important for the measurement of accurate p_E and k_{ex} values in cases where fields of only a few Hz are used (Figure S3). We recommend focusing on a single, intense, well resolved peak in the 2D $^{15}N-^1H$ HSQC data set using a selective $^1H-^{15}N$ heteronuclear Hartmann−Hahn scheme (see legend to Figure 1),[60,61] with the size of the CEST B_1 field obtained using the nutation approach of Guenneugues et al.,[38] except that DANTE rather than CW excitation is performed, Figure 1B, as in the actual experiment. However, in the standard calibration scheme the resulting signal has a $\cos(\omega_1 t)$ modulation so that a pair of peaks are produced that are separated by twice the weak B_1 field strength ($\omega_1 = 2\pi B_1$). In cases where the B_1 is very weak (only a few Hz), the doublet nature of the spectrum, and the resulting overlap of the two components, leads to an underestimation of the field. In these cases we prefer, therefore, to record both quadrature components so that only a single peak at the frequency of the B_1 field is present, as described in the caption for Figure 1 and in Supporting Information.

Theoretical Considerations. In what follows we briefly outline the approach used to extract solvent exchange rates from ^{15}N D-CEST data. From eq 1 we can write a system of equations that describes the evolution of exchanging magnetization during the course of a pulse of duration τ_p and strength ω_1 (rad/s) using the Bloch−McConnell equations[62] as

DOI: 10.1021/acs.jpcb.8b06820
J. Phys. Chem. B 2018, 122, 11206−11217

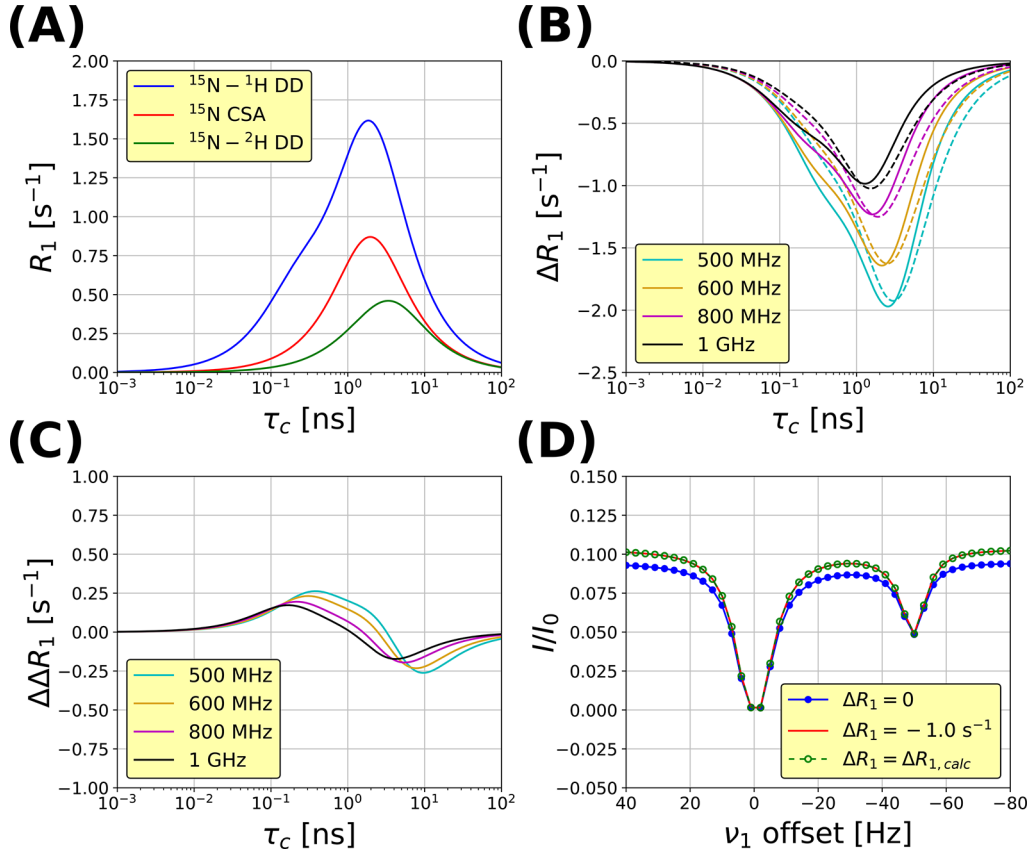

Figure 2. (A) Contributions of ^{15}N–^{1}H dipolar (DD), ^{15}N CSA, and ^{15}N–^{2}H dipolar relaxation interactions to backbone amide ^{15}N R_1 rates as a function of rotational correlation time, τ_c, 800 MHz. An axially symmetric CSA tensor of magnitude −160 ppm is assumed, along with an ^{15}N–^{1}H(^{2}H) bond length of 1.02 Å.[72,74,75] S^2 is set to 1 in all simulations. (B) $\Delta R_1 = R_{1,N_D} - R_{1,N_H}$ as a function of τ_c, as calculated from eqs 7−9, $S^2 = 1$ (continuous curves), or $\Delta R_{1,calc}=(\eta - 1)R_{1,N_H}$, $\eta = \frac{R_{1,N_D}}{R_{1,N_H}}$, that is optimized for each field (dashed curves). (C) $\Delta\Delta R_1 = \Delta R_{1,calc} - \Delta R_1$, evaluated using optimized η values for each field, as a function of τ_c. The optimal value of η is chosen in order to minimize the largest value of $|\Delta\Delta R_1| = |\Delta R_1 - \Delta R_{1,calc}|$; values of 0.38, 0.42, 0.50, or 0.57 are obtained for 500, 600, 800, or 1000 MHz, respectively. (D) Simulated ^{15}N D-CEST profiles, 800 MHz, calculated (i, blue) with $\Delta R_1 = 0$ s^{-1}, (ii, red) with $R_{1,E}(R_{1,N_D}) = 1.25$ s^{-1}, $R_{1,G}(R_{1,N_H}) = 2.25$ s^{-1} so that $\Delta R_1 = -1.0$ s^{-1}, and (iii, green dashed) with $R_{1,G}(R_{1,N_H}) = 2.25$ s^{-1} and by assuming $\Delta R_1 = \Delta R_{1,calc}$ ($\eta = 0.50$) = −1.13 s^{-1}. The R_1 and ΔR_1 rates were calculated from eqs 7−9, assuming $\tau_c = 3$ ns, $S^2 = 1$. Additional simulation parameters are $R_{2,G} = R_{2,E} = 5$ s^{-1}, $T_{Ex} = 1$ s, $B_1 = 3$ Hz, $k_{ex} = 10$ s^{-1}, $p_E = 10\%$, and $\Delta\nu_{GE} = -50$ Hz.

$$\frac{d}{dt}\begin{bmatrix} N_x^H(t) \\ N_y^H(t) \\ N_z^H(t) \\ N_x^D(t) \\ N_y^D(t) \\ N_z^D(t) \end{bmatrix} = \begin{bmatrix} -R_{2,N_H} - P_D k_{HD} & -\omega_{N_H} & 0 & P_H k_{DH} & 0 & 0 \\ \omega_{N_H} & -R_{2,N_H} - P_D k_{HD} & -\omega_1 & 0 & P_H k_{DH} & 0 \\ 0 & \omega_1 & -R_{1,N_H} - P_D k_{HD} & 0 & 0 & P_H k_{DH} \\ P_D k_{HD} & 0 & 0 & -R_{2,N_D} - P_H k_{DH} & -\omega_{N_D} & 0 \\ 0 & P_D k_{HD} & 0 & \omega_{N_D} & -R_{2,N_D} - P_H k_{DH} & -\omega_1 \\ 0 & 0 & P_D k_{HD} & 0 & \omega_1 & -R_{1,N_D} - P_H k_{DH} \end{bmatrix} \begin{bmatrix} N_x^H(t) \\ N_y^H(t) \\ N_z^H(t) \\ N_x^D(t) \\ N_y^D(t) \\ N_z^D(t) \end{bmatrix} \quad (2)$$

where k_{DH} and k_{HD} are the solvent exchange rates measured in solutions of 100% H_2O or 100% D_2O, respectively, and $R_{2,N_H}(R_{2,N_D})$ is the ^{15}N transverse relaxation rate for a protonated(deuterated) amide with the corresponding longitudinal rate denoted by $R_{1,N_H}(R_{1,N_D})$. The evolution during each of the delays between pulses is simply given by the above expression with $\omega_1 = 0$. It is assumed that only ^{15}N magnetization from NH (and not ND) is present at the start of the CEST delay and that the detected signal derives from NH.

In what follows we have fit the resulting CEST profiles to obtain residue-specific k_{ex}, $\Delta\varpi = \varpi_{N_D} - \varpi_{N_H}$, and relaxation rates, as well as the global parameter p_E. From detailed balance it follows that

$$p_G P_D k_{HD} = p_E P_H k_{DH} \quad (3)$$

and hence

$$\phi = \frac{k_{HD}}{k_{DH}} = \frac{p_E P_H}{p_G P_D} = \frac{p_E(1 - P_D)}{(1 - p_E)P_D} \quad (4)$$

DOI: 10.1021/acs.jpcb.8b06820
J. Phys. Chem. B 2018, 122, 11206−11217

where ϕ is the fractionation factor,[63] corresponding to the relative fraction of ND vs NH at a site when $P_H = P_D = 0.5$. It follows that

$$k_{ex} = P_D k_{HD} + P_H k_{DH} = (P_D(\phi - 1) + 1)k_{DH} \quad (5)$$

and

$$p_E = \frac{\phi P_D}{1 + P_D(\phi - 1)} \quad (6)$$

A value of $\phi = 1.1$ has been reported for amides in a random coil configuration,[64,65] while LiWang and Bax have measured ϕ values ranging from 1.01 to 1.21 for ubiquitin.[65] For $\phi \sim 1.1$, as is the case for unfolded proteins, and most likely for most residues in folded proteins as well, k_{ex} and p_E are well approximated by $k_{ex} = (0.1P_D + 1)k_{DH}$ and $p_E = 1.1P_D/(1 + 0.1P_D)$ and for small values of P_D, as used here (~10%), $k_{ex} \simeq k_{DH}$ and $p_E \simeq 1.1P_D$.

As described above we have treated p_E as a global fitting parameter. This is not optimal in cases where ϕ values are expected to vary significantly between residues (eq 6). Instead, it is possible to first estimate ϕ values from residue-specific p_E values that are obtained from fits of the CEST profiles and P_D that is accurately known so long as samples are careful prepared (eq 4) and, subsequently, to obtain k_{DH} from fitted k_{ex} values and ϕ (eq 5). Alternatively, ϕ values can be obtained independently[23,65] and then used to extract k_{DH} (eqs 4 and 5). It is worth mentioning that the measured k_{DH} values must be adjusted for a kinetic isotope effect before direct comparison with hydrogen exchange rates that quantify the interchange of protons at NH positions, such as those obtained via CLEANEX- or WEX-type experiments,[12,20] but this is easily accomplished using literature values ($k_{HH}/k_{DH} \sim 1.20$ at pH 6.5, 30 °C)[66,67] or the *SPHERE* server on the Web.[68]

In CEST applications from our laboratory we have always assumed that longitudinal relaxation rates in the ground and excited states were equivalent, as simulations had shown that this assumption introduces little error in the extracted exchange parameters.[29,30] However, because we are particularly interested in obtaining k_{ex} rates that are as accurate as possible here, we have examined this problem further, considering only differences in ^{15}N relaxation rates that arise from the presence of a coupled ^1H or ^2H.

Expressions for ^{15}N relaxation in isolated $^{15}N-^1H$ and $^{15}N-^2H$ spin pairs can be readily calculated as[50]

$$R_{1,DD}^{N-H} = \frac{1}{4}\left(\frac{\mu_0 \hbar \gamma_H \gamma_N}{4\pi r_{NH}^3}\right)^2 [J(\omega_N - \omega_H) + 3J(\omega_N) + 6J(\omega_N + \omega_H)] \quad (7)$$

$$R_{1,DD}^{N-D} = \frac{2}{3}\left(\frac{\mu_0 \hbar \gamma_D \gamma_N}{4\pi r_{ND}^3}\right)^2 [J(\omega_N - \omega_D) + 3J(\omega_N) + 6J(\omega_N + \omega_D)] \quad (8)$$

$$R_{1,CSA} = \left(\frac{\Delta\sigma\omega_N}{\sqrt{3}}\right)^2 J(\omega_N) \quad (9)$$

where the subscripts DD and CSA refer to contributions to relaxation from dipole−dipole and chemical shift anisotropy relaxation mechanisms. The spectral density $J(\omega)$ is defined as[69,70]

$$J(\omega) = \frac{2}{5}\left(\frac{S^2\tau_c}{1 + (\omega\tau_c)^2} + \frac{(1 - S^2)\tau}{1 + (\omega\tau)^2}\right) \quad (10)$$

τ_c is the correlation time of the assumed isotropic overall rotation, $\tau^{-1} = \tau_c^{-1} + \tau_e^{-1}$, S^2 is the square of an order parameter quantifying the amplitude of the amide bond vector motion, τ_e is an effective correlation time of bond vector motion, γ_i is the gyromagnetic ratio of spin i, r_{kl} is the distance between spins k and l (set to 1.02 Å), and $\Delta\sigma$ is the ^{15}N chemical shift anisotropy (−160 ppm[71,72]). The calculated R_1 contribution from each relaxation source at 800 MHz is shown in Figure 2A. The difference in R_1 rates, $\Delta R_1 = R_{1,N_D} - R_{1,N_H}$, as a function of τ_c is illustrated in Figure 2B for the case where $S^2 = 1$ (solid lines); values of $S^2 < 1$ lead to smaller ΔR_1 differences. Since it is typically difficult to measure R_{1,N_D}[73,74] we choose to include ΔR_1 in fits of CEST data by assuming magnetic field dependent ratios $\eta = \frac{R_{1,N_D}}{R_{1,N_H}}$, which are taken to be constant over all motional parameters (*i.e.*, for all τ_c, S^2, τ_e). With this assumption it follows that $\Delta R_{1,calc} = (\eta - 1)R_{1,N_H}$ and additional fitting parameters are not required (beyond R_{1,N_H}). Optimal values for η were chosen by minimizing the largest $|\Delta\Delta R_1|$ value for each magnetic field, with $\Delta\Delta R_1 = \Delta R_{1,calc} - \Delta R_1$. Values of $\Delta R_{1,calc}$ obtained with the optimized η values are also shown in Figure 2B (dashed lines), along with $\Delta\Delta R_1$ rates in Figure 2C. Figure 2D compares simulated CEST profiles obtained with $k_{ex} = 10\ s^{-1}$, $p_E = 10\%$, and $\Delta R_1 = 0\ s^{-1}$ (blue) or $-1.0\ s^{-1}$ (red). The larger effective minor dip size (relative to baseline) in the case where $\Delta R_1 = -1.0\ s^{-1}$ translates into errors in k_{ex} (+0.3 s^{-1}) and p_E (+1.1%) when ΔR_1 is set to 0 in the fit. However, when ΔR_1 is calculated as $(\eta - 1)R_{1,N_H}$, accurate k_{ex} and p_E values are extracted and the resultant CEST profile (dashed green line) matches the one obtained with $\Delta R_1 = -1.0\ s^{-1}$.

As a further test we have simulated D-CEST profiles using R_{1,N_H} and R_{1,N_D} rates calculated (800 MHz) with τ_c, S^2, and τ_e values in the ranges $1\ ns \le \tau_c \le 100\ ns$, $0 \le S^2 \le 1$, and $1\ ps \le \tau_e < 100\ ps$, with $10\ s^{-1} \le k_{ex} \le 100\ s^{-1}$, $0 \le p_E \le 0.5$. Simulated profiles were obtained using two different weak B_1 fields of 3 and 5 Hz, $T_{Ex} = 1$ s, and subsequently fit together using $\eta = 0.50$ (see legend to Figure 2 that lists optimal η values). In all cases the examined error in k_{ex} does not exceed 0.1 s^{-1}. Thus, this approach of estimating ΔR_1 provides a simple and effective way of taking into account differences in relaxation of ^{15}N longitudinal magnetization from NH and ND states in fits of CEST data.

Typically, in most applications, differences in transverse relaxation rates of spins in states G and E are subsumed in an extra fitting parameter, ΔR_2. In the present set of applications, where solvent exchange is quantified, ΔR_2 values can be predicted to good accuracy by taking into account differences in relaxation rates between isolated $^{15}N-^1H$ and $^{15}N-^2H$ spin pairs. In the slow tumbling limit, where $\Delta R_2/R_{2,G}$ does not depend significantly on τ_c, R_2 is proportional to $J(0)$ and $\Delta R_2/R_{2,G} = -0.77$ (500 MHz), −0.71 (600 MHz), −0.60 (800 MHz), and −0.50 (1 GHz). Solvent exchange rates that we have obtained by either keeping $\Delta R_2/R_{2,G}$ fixed to the values above or by fitting ΔR_2 directly are consistent.

Experimental Applications. Most CEST applications involve states that interconvert with rates in excess of 100 s^{-1}, and in these cases, B_1 fields on the order of, or larger than, approximately 20 Hz are optimal.[42] It is straightforward to

DOI: 10.1021/acs.jpcb.8b06820
J. Phys. Chem. B 2018, 122, 11206−11217

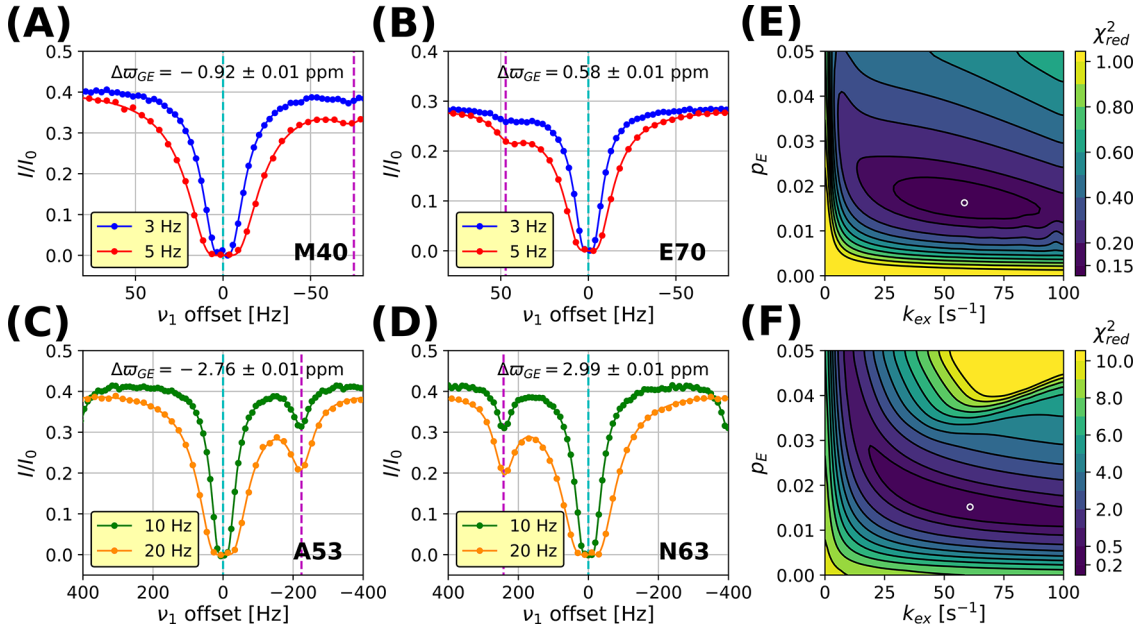

Figure 3. ^{15}N D-CEST profiles from representative residues in the A39G FF domain, 1 °C and 800 MHz. (A–D) D-CEST profiles measured with weak B_1 fields of 3 and 5 Hz (A, B) or 10 and 20 Hz (C, D). A circular shift has been performed for each D-CEST profile such that the ground state position is placed at $\nu_1 = 0$ (cyan dashed line), exploiting the periodic nature of the profiles (*i.e.*, profiles repeat every sw_{CEST}).[31,32] The excited state position, corresponding to the resonance position of the spin in the unfolded state, is indicated by the magenta dashed line in each plot. (E, F) χ^2 surface plots based on fits of D-CEST profiles measured with (E) 3 and 5 Hz and (F) 10 and 20 Hz B_1 fields.There are 10 and 28 residues with well resolved minor dips included in each global fit in panels E and F, respectively. Values of (p_E, k_{ex}) at the global χ^2 minimum of each plot are indicated by the white circles; values of (1.63 ± 0.03%, 58.4 ± 2.9 s^{-1}) and (1.52 ± 0.01%, 60.8 ± 1.2 s^{-1}) are obtained in panels E and F, respectively.

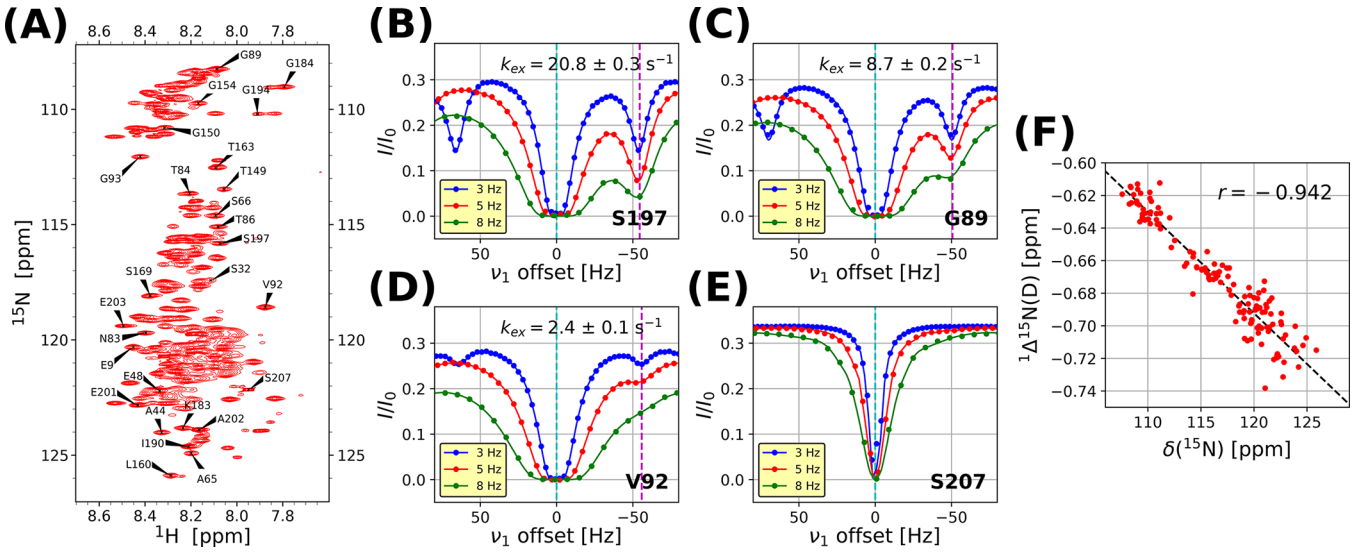

Figure 4. (A) ^{1}H–^{15}N correlation map of Ddx4$_{cond}$, 30 °C, 800 MHz, with selected peak assignments,[35] as indicated. (B–E) ^{15}N D-CEST profiles from several representative residues in Ddx4$_{cond}$. A circular shift of the data has been applied, placing the ground state position in the center of each spectral window (cyan dashed line); the position of the excited state is indicated by the magenta dashed line in each plot (omitted for panel E where solvent exchange is too slow to observe a minor state dip <0.5 s^{-1}). Note that sw_{CEST} values of 120, 150, and 160 Hz have been used for CEST profiles recorded with B_1 fields of 3, 5, and 8 Hz, respectively. As described in detail previously,[31] the use of such small sw_{CEST} values, in general, creates an ambiguity in the position of the excited state resonance ($\nu_E \pm sw_{CEST}$) for each B_1 field (that can be eliminated when multiple sw_{CEST} measurements are obtained[31]). This is indicated for the 3 Hz profiles (blue curves) where a second "false" minor dip is observed downfield of the major state dip that results from aliasing. For the profiles recorded with the larger B_1 fields, the displayed region (±80 Hz) is not sufficiently large to show the aliased dips. However, this ambiguity is not an issue here: (i) the smallest common multiple of the 3 sw_{CEST} values used is 2400 Hz = 30 ppm, and as profiles from all 3 fields are simultaneously fit for each residue the effective ambiguity in the position of the minor state peak is 30 ppm, larger than the range of ^{15}N shifts and (ii) as the one-bond ^{2}H isotope shift is known for ^{15}N, this ambiguity is not relevant in the present study. (F) Correlation of $\Delta\varpi_{GE} = {}^1\Delta^{15}$N(D) for Ddx4$_{cond}$ obtained from ^{15}N D-CEST vs ^{15}N chemical shifts (^{15}N–^{1}H amides). The slope of the best-fitting line is −0.0062 based on 138 residues.

calibrate such fields in an accurate manner, and homo- or heteronuclear couplings to the probe spins of interest that are not decoupled during the CEST interval can be easily taken into account in data analysis,[36,76] although often this is not necessary.

DOI: 10.1021/acs.jpcb.8b06820
J. Phys. Chem. B 2018, 122, 11206–11217

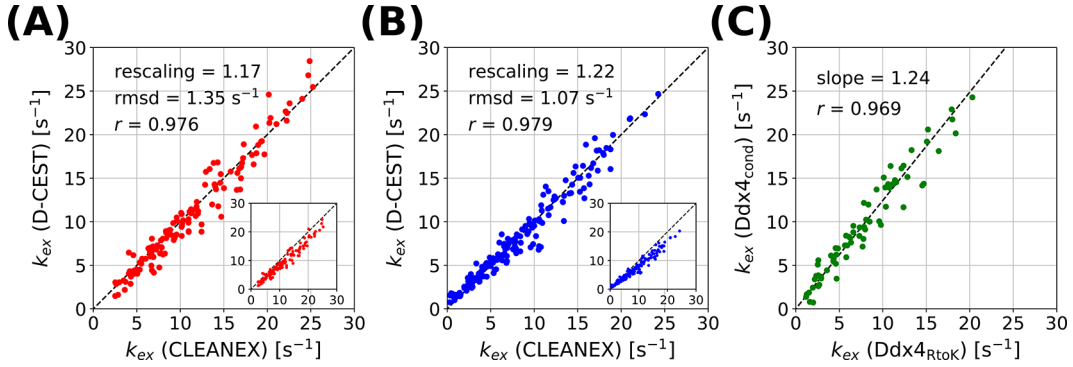

Figure 5. Correlation of solvent exchange rates, k_{ex}, obtained from ^{15}N D-CEST and CLEANEX-PM measurements recorded on (A) Ddx4$_{cond}$ and (B) Ddx4$_{RtoK}$ samples. In each case, k_{ex} rates from D-CEST are multiplied by rescaling factors (1.17 and 1.22 for panels A and B, respectively) that minimize root-mean-square-differences (rmsd) between values measured with D-CEST and CLEANEX-PM, as described in the text. Note that these factors are consistent with the ratio between k_{HH} and k_{DH} solvent exchange rates that are measured on model systems,[67] see text. The insets show the correlation prior to rescaling the exchange rates measured via D-CEST. (C) Linear correlation plot of k_{ex} values from ^{15}N D-CEST measured on Ddx4$_{cond}$ and Ddx4$_{RtoK}$ samples. The slope of 1.24 likely reflects slightly different sample conditions. The data sets in panels A−C include 138, 178, and 72 residues, respectively.

In contrast, when fields on the order of a few Hz are used there are concerns about how even small couplings might influence both calibration and analysis, as well as how B_1 inhomogeneity might affect the accuracy of the extracted exchange parameters. As a first test to evaluate whether accurate exchange parameters can be isolated when fields on the order of 3−5 Hz are used, we have focused on an A39G FF domain sample that has been previously shown to exchange between a ground state folded conformation and a sparse ensemble of unfolded structures.[77] We have used a fully protonated sample to test the robustness of the ^{1}H decoupling field during the CEST interval in the presence of heteronuclear $^2J_{HN}$ and $^3J_{HN}$ couplings. Figure 3A−D highlights a number of representative CEST profiles recorded on this sample, 800 MHz and 1 °C, using B_1 fields of 3, 5, 10, and 20 Hz that illustrate the increase in line widths with B_1 field. Best fit exchange parameters, (p_E, k_{ex}), obtained from independent analyses of profiles from the two "strong" (10 and 20 Hz) or the two "weak" B_1 fields (3 and 5 Hz), are (1.52 ± 0.01%, 60.8 ± 1.2 s^{-1}) and (1.63 ± 0.03%, 58.4 ± 2.9 s^{-1}), respectively. Further, χ^2 surfaces, plotting (p_E, k_{ex}) values for each of the fits are consistent, Figure 3E,F, confirming that accurate exchange parameters can be obtained in studies on protonated samples even when very weak B_1 fields are used.

We next measured solvent hydrogen exchange rates in a phase-separated sample of the intrinsically disordered domain of Ddx4, Ddx4$_{cond}$,[34,35,78] Figure 4A. We have previously shown that the condensed phase of the phase-separated Ddx4 domain is highly viscous with individual molecules diffusing with rates expected for a particle with a 600 nm hydrodynamic radius.[35] However, sharp resonances are observed in the spectra (Figure 4A), consistent with extensive local dynamics. ^{15}N D-CEST profiles were recorded using weak B_1 fields of 3, 5, and 8 Hz and T_{Ex} = 1 s, as shown for selected residues in Figure 4B−E. Initially, a global fit of the data was performed using 10 residues with the largest minor state CEST dip sizes, and a value of p_E = 9.5 ± 0.1% was obtained that is in keeping with expectations, as approximately 10% D_2O was added to the buffer. Notably, k_{ex} values obtained from fits of 3 and 5 Hz data sets are in excellent agreement with rates quantified from analysis of all three B_1 fields. The extracted $\Delta\varpi_{GE}$ (=$^1\Delta^{15}$N(D)) values show a good correlation with ground state ^{15}N chemical shifts, as has been observed previously for residues in disordered regions of ubiquitin,[79] Figure 4F.

We have validated the k_{ex} rates obtained using the ^{15}N D-CEST approach by measuring a second set of solvent exchange values with the CLEANEX-PM scheme[20] recorded on Ddx4$_{cond}$ (Figure S4). As discussed above, in the ^{15}N D-CEST experiment, and for P_D ∼ 10% and $\phi \simeq 1.1$, as is the case for disordered proteins, $k_{ex} \simeq k_{DH}$, where k_{DH} is the ND to NH exchange rate in a ^1H_2O solution. In contrast, k_{ex} values obtained via the CLEANEX-PM approach correspond to hydrogen exchange for NH amides in ^1H_2O solvent (k_{HH}). Englander and co-workers measured k_{HH}/k_{DH} ∼ 1.20 for base catalysis of hydrogen exchange in poly-DL-alanine at 20 °C,[67] and this group provides software from which residue-specific k_{HH}/k_{DH} values can be calculated.[80] Figure 5A shows a correlation plot between k_{ex} values from D-CEST (y-axis) and CLEANEX-PM (x-axis) before (inset) and after (main plot) multiplication of the D-CEST data to minimize the difference in rates from the two methods. Notably, k_{HH} = 1.17 × k_{DH} (inset) in excellent agreement with the poly-DL-alanine data and with expectations based on calculations using software from the Englander laboratory[80] that specifically takes into account the conditions under which the exchange reaction was performed.

We have repeated the analysis using a sample of Ddx4$_{RtoK}$ that does not phase separate (Figures S5 and S6),[35] and as with phase-separated Ddx4$_{cond}$, an excellent correlation between k_{HH} and k_{DH} is obtained, k_{HH} = 1.22 × k_{DH} (inset), Figure 5B. Finally, k_{ex} values measured for Ddx4$_{cond}$ and Ddx4$_{RtoK}$ are highly correlated, Figure 5C, although the increased rates for Ddx4$_{cond}$ most likely reflect a slightly higher pH (∼0.08 units) in this sample, and perhaps also differences in primary sequence associated with the Arg to Lys mutations. The fact that similar solvent hydrogen exchange rates are measured for Ddx4$_{cond}$ and Ddx4$_{RtoK}$ samples implies that the primary contributor to phase separation cannot be extensive interactions involving amide groups within or between protein molecules in the phase-separated state that would sequester the amides from solvent.

Optimal P_D/P_H Values. In the examples presented above we have studied exchange in systems where the buffer composition is ∼10% D_2O/∼90% H_2O (P_D ∼ 10%). P_D values on the order of 5−10% are typical for NMR samples that are used for a variety of different experiments, so that hydrogen exchange via D-CEST

DOI: 10.1021/acs.jpcb.8b06820
J. Phys. Chem. B 2018, 122, 11206−11217

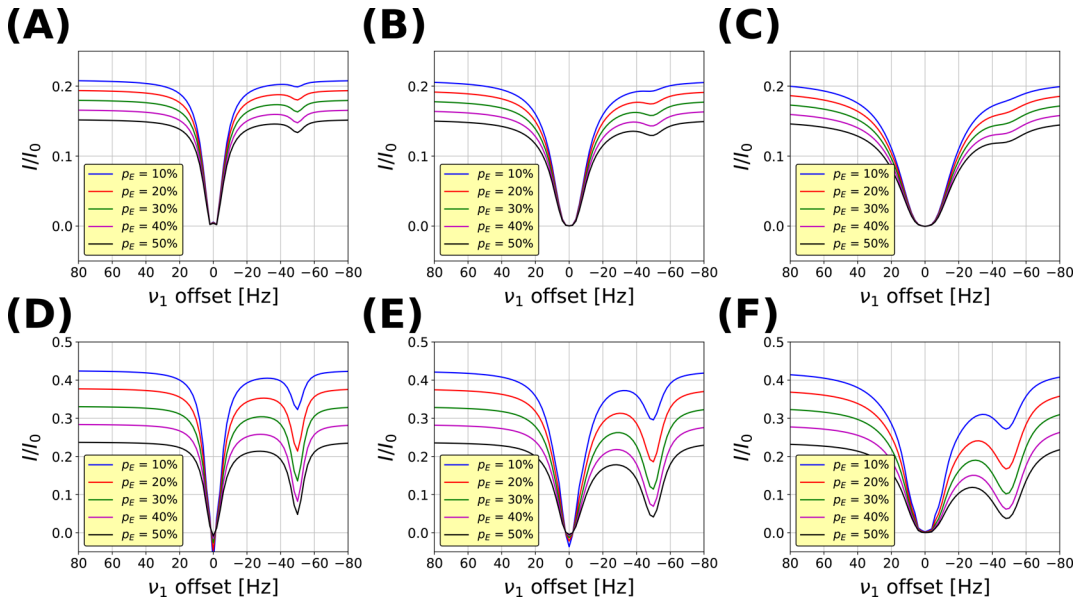

Figure 6. Effect of increasing the fractional amount of D_2O on ^{15}N D-CEST profiles reporting on solvent hydrogen exchange. The parameters used in the simulations are $R_{1,G} = R_{1,E} = 1.5\ s^{-1}$, $R_{2,G} = R_{2,E} = 5\ s^{-1}$, $\Delta\nu_{GE} = -50$ Hz, and (A−C) $T_{Ex} = 1$ s or (D−F) $T_{Ex} = 500$ ms. Panels A−C or D−F are simulated with $B_1 = 3$ (A, D), 5 (B, E), and 8 (C, F) Hz, respectively. A value of $k_{ex} = 1\ s^{-1}$ is used for panels A−C, and $10\ s^{-1}$ for panels D−F, and it is assumed that $\phi = 1$ so that $p_E = P_D$.

can be measured without the need for a "special sample". Because the CEST experiment amplifies the signal from the rare state, in this case from amides that are deuterated, the small p_E values that ensue need not be a deterrent, and accurate k_{ex} rates can be obtained (see above). It is of interest to examine whether there are advantages in pursuing higher P_D values, as then p_E will be scaled accordingly (eq 6) and larger dips in CEST profiles would be obtained. The optimal D_2O/H_2O fraction depends, to a large extent, on the k_{ex} values that are to be measured and on the inherent sensitivity of the spectra that are recorded, and it is not immediately obvious that large values of P_D should be used. For example, the rate of solvent exchange from NH to ND increases in proportion to P_D, decreasing the efficiency of magnetization transfer during the pulse scheme and hence the resulting signal-to-noise of data sets. If exchange rates are inherently high ($50-100\ s^{-1}$) it is advantageous to work with samples with low P_D values; in contrast, for amides that exchange much more slowly, higher P_D values may be beneficial. However, as the signal originates from NH amides whose concentration decreases in proportion to P_D, the inherent sensitivity of spectra decreases with solvent deuteration levels. Further, as the exchange from NH to ND during the CEST period ultimately leads to a decrease in net observable magnetization, the baselines of CEST profiles decrease with P_D, further lowering the inherent sensitivity of the measurement. This is illustrated in Figure 6 where CEST profiles as a function of P_D are shown for a very slowly exchanging amide proton ($k_{ex} = 1\ s^{-1}$) and one with a moderate exchange rate ($10\ s^{-1}$). So long as sensitivity is high and k_{ex} is small, the gain in the sizes of minor state dips will likely offset the disadvantages of using higher P_D values. More generally, as a range of k_{ex} rates is likely to be present, we recommend using small P_D values, at least in initial measurements.

^{15}N D-CEST vs CLEANEX-PM for Measurement of Solvent Hydrogen Exchange. The development of multifrequency excitation schemes provides an avenue for the use of very weak B_1 fields in CEST studies that otherwise are prohibitive in terms of measurement times. One of a number of potential applications that is now possible is the measurement of solvent hydrogen exchange rates, as described above. In the D-CEST approach, exchange rates can be quantified directly from CEST profiles recorded with different B_1 fields, and as ^{15}N magnetization is evolved during the CEST exchange period the relaxation behavior is relatively "simple" to analyze. An accurate evaluation of R_{1,N_D} is required, but that can be obtained simply from R_{1,N_H} that is a fitting parameter. A limitation of the method is that it requires reasonably well resolved minor state dips, placing an upper bound on measured k_{ex} values of $\sim 100\ s^{-1}$. In contrast, other approaches that quantify exchange through initial perturbation of the water resonance must separate solvent exchange from magnetization exchange (^1H cross-relaxation) processes.[12,16,20] In the CLEANEX-PM method used here this is achieved via application of a multipulse spin-lock scheme during the mixing period so that cross-relaxation between pairs of proximal proton spins is averaged to zero, assuming that tumbling is in the macromolecular limit. For applications to unfolded proteins it would be expected that this approach would be less effective as the condition of slow tumbling is unlikely to be fulfilled. Nevertheless, the close agreement between k_{ex} rates obtained via D-CEST and CLEANEX-PM (Figure 5) suggests that cross-relaxation is well suppressed in the Ddx4 systems studied here. Notably, however, the CLEANEX-PM mixing scheme places magnetization in the transverse plane for 1/3 of the exchange period so that the relaxation losses during this interval can be quite significant if the systems studied are large. For example, for $Ddx4_{cond}$ the measured average ^1H relaxation rate during this delay is $\sim 30\ s^{-1}$ (Figure S7). Bax and co-workers have developed a TROSY-based WEX-III scheme for hydrogen exchange measurements on high molecular weight protein systems to circumvent this problem and applied it to a 36 kDa deuterated homodimer of the integrase catalytic core domain.[12] The ^{15}N CEST approach demonstrated here can also be used to study exchange in higher molecular weight proteins as ^{15}N R_1 relaxation rates scale inversely with size, and, moreover,

DOI: 10.1021/acs.jpcb.8b06820
J. Phys. Chem. B 2018, 122, 11206−11217

inversely with the square of the Larmor frequency, so that higher magnetic fields are also beneficial.

CONCLUSIONS

Here we have demonstrated the utility of ^{15}N D-CEST for quantifying solvent hydrogen exchange rates in ^{15}N-labeled proteins. Central to the method is a multifrequency excitation scheme, enabling the use of very weak B_1 fields without the concomitant significant increase in measurement time that would otherwise accompany CEST experiments based on continuous wave excitation. An advantage of D-CEST is that the method is based on quantitation of ^{15}N relaxation, and unlike approaches in which the water resonance is selectively perturbed, the complexities of ^{1}H relaxation do not enter into the analysis. A first application to the study of chemical exchange in a small FF domain that interconverts between folded and unfolded conformations establishes that accurate exchange parameters can be measured when very weak B_1 fields are used. Solvent hydrogen exchange rates measured on a phase-separated Ddx4 domain as well as on a variant of the protein that does not phase separate using the D-CEST approach are in excellent agreement with values obtained via CLEANEX-PM, further validating the approach. It is anticipated that multifrequency CEST excitation, in general, will enable a variety of different studies where resolution in CEST profiles is critical and, as such, will serve as a useful addition to an increasingly growing set of CEST-based tools for investigating rare protein states.

ASSOCIATED CONTENT

Supporting Information

The Supporting Information is available free of charge on the ACS Publications website at DOI: 10.1021/acs.jpcb.8b06820.

Additional discussion of ^{15}N D-CEST experiment including weak ^{15}N B_1 field calibration and ^{1}H/^{2}H decoupling schemes, CLEANEX-PM experimental details and data fitting results, pulse sequence code, and Figures S1−S7 (PDF)

AUTHOR INFORMATION

Corresponding Author

*E-mail: kay@pound.med.utoronto.ca. Phone: 416-978-0741. Fax: 416-978-6885.

ORCID

Tairan Yuwen: 0000-0003-3504-7995

Fabien Ferrage: 0000-0002-4738-1723

Lewis E. Kay: 0000-0002-4054-4083

Present Address

[▽]Department of Biochemistry and Molecular Biology, SUNY Upstate Medical University, Syracuse, New York 13210, United States (A.B.).

Notes

The authors declare no competing financial interest.

ACKNOWLEDGMENTS

This work was supported by a grant from the Canadian Institutes of Health Research (CIHR) to L.E.K. and with financial support from the French National Center for Scientific Research to G.B. T.Y. acknowledges postdoctoral support from the CIHR. L.E.K. holds a Canada Research Chair in Biochemistry. This paper is dedicated to Dr. Bill Eaton on the occasion of his 80th birthday with great respect and admiration.

REFERENCES

(1) Hvidt, A.; Nielsen, S. O. In *Advances in Protein Chemistry*; Anfinsen, C. B., Anson, M. L., Edsall, J. T., Richards, F. M., Eds.; Academic Press: London, U.K., 1966; Vol. *21*, pp 287−386.

(2) Englander, S. W.; Mayne, L.; Bai, Y.; Sosnick, T. R. Hydrogen Exchange: The Modern Legacy of Linderstrøm-Lang. *Protein Sci.* **1997**, *6*, 1101−1109.

(3) Karplus, M.; Kuriyan, J. Molecular Dynamics and Protein Function. *Proc. Natl. Acad. Sci. U. S. A.* **2005**, *102*, 6679−6685.

(4) Eisenmesser, E. Z.; Millet, O.; Labeikovsky, W.; Korzhnev, D. M.; Wolf-Watz, M.; Bosco, D. A.; Skalicky, J. J.; Kay, L. E.; Kern, D. Intrinsic Dynamics of an Enzyme Underlies Catalysis. *Nature* **2005**, *438*, 117−121.

(5) Sekhar, A.; Kay, L. E. NMR Paves the Way for Atomic Level Descriptions of Sparsely Populated, Transiently Formed Biomolecular Conformers. *Proc. Natl. Acad. Sci. U. S. A.* **2013**, *110*, 12867−12874.

(6) Kimsey, I. J.; Szymanski, E. S.; Zahurancik, W. J.; Shakya, A.; Xue, Y.; Chu, C. C.; Sathyamoorthy, B.; Suo, Z. C.; Al-Hashimi, H. M. Dynamic Basis for dG.dT Misincorporation via Tautomerization and Ionization. *Nature* **2018**, *554*, 195−201.

(7) Mayo, S. L.; Baldwin, R. L. Guanidinium Chloride Induction of Partial Unfolding in Amide Proton Exchange in RNase A. *Science* **1993**, *262*, 873−876.

(8) Bai, Y. W.; Sosnick, T. R.; Mayne, L.; Englander, S. W. Protein Folding Intermediates: Native-State Hydrogen Exchange. *Science* **1995**, *269*, 192−197.

(9) Lee, T.; Hoofnagle, A. N.; Kabuyama, Y.; Stroud, J.; Min, X. S.; Goldsmith, E. J.; Chen, L.; Resing, K. A.; Ahn, N. G. Docking Motif Interactions in MAP Kinases Revealed by Hydrogen Exchange Mass Spectrometry. *Mol. Cell* **2004**, *14*, 43−55.

(10) Lührs, T.; Ritter, C.; Adrian, M.; Riek-Loher, D.; Bohrmann, B.; Döbeli, H.; Schubert, D.; Riek, R. 3D Structure of Alzheimer's Amyloid-β(1−42) Fibrils. *Proc. Natl. Acad. Sci. U. S. A.* **2005**, *102*, 17342−17347.

(11) Lu, X. J.; Wintrode, P. L.; Surewicz, W. K. β-Sheet Core of Human Prion Protein Amyloid Fibrils As Determined by Hydrogen/Deuterium Exchange. *Proc. Natl. Acad. Sci. U. S. A.* **2007**, *104*, 1510−1515.

(12) Fitzkee, N. C.; Torchia, D. A.; Bax, A. Measuring Rapid Hydrogen Exchange in the Homodimeric 36 kDa HIV-1 Integrase Catalytic Core Domain. *Protein Sci.* **2011**, *20*, 500−512.

(13) Englander, S. W.; Downer, N. W.; Teitelbaum, H. Hydrogen Exchange. *Annu. Rev. Biochem.* **1972**, *41*, 903−924.

(14) Arrington, C. B.; Robertson, A. D. Kinetics and Thermodynamics of Conformational Equilibria in Native Proteins by Hydrogen Exchange. *Methods Enzymol.* **2000**, *323*, 104−124.

(15) Spera, S.; Ikura, M.; Bax, A. Measurement of the Exchange Rates of Rapidly Exchanging Amide Protons: Application to the Study of Calmodulin and Its Complex with a Myosin Light Chain Kinase Fragment. *J. Biomol. NMR* **1991**, *1*, 155−165.

(16) Grzesiek, S.; Bax, A. Measurement of Amide Proton Exchange Rates and NOEs with Water in ^{13}C/^{15}N-Enriched Calcineurin-B. *J. Biomol. NMR* **1993**, *3*, 627−638.

(17) Gemmecker, G.; Jahnke, W.; Kessler, H. Measurement of Fast Proton Exchange Rates in Isotopically Labeled Compounds. *J. Am. Chem. Soc.* **1993**, *115*, 11620−11621.

(18) Mori, S.; Johnson, M. O.; Berg, J. M.; van Zijl, P. C. M. Water Exchange Filter (WEX Filter) for Nuclear Magnetic Resonance Studies of Macromolecules. *J. Am. Chem. Soc.* **1994**, *116*, 11982−11984.

(19) Hwang, T. L.; Mori, S.; Shaka, A. J.; van Zijl, P. C. M. Application of Phase-Modulated CLEAN Chemical EXchange Spectroscopy (CLEANEX-PM) to Detect Water−Protein Proton Exchange and Intermolecular NOEs. *J. Am. Chem. Soc.* **1997**, *119*, 6203−6204.

(20) Hwang, T. L.; van Zijl, P. C. M.; Mori, S. Accurate Quantitation of Water−Amide Proton Exchange Rates Using the Phase-Modulated CLEAN Chemical EXchange (CLEANEX-PM) Approach with a Fast-HSQC (FHSQC) Detection Scheme. *J. Biomol. NMR* **1998**, *11*, 221−226.

(21) Rennella, E.; Solyom, Z.; Brutscher, B. Measuring Hydrogen Exchange in Proteins by Selective Water Saturation in ^{1}H−^{15}N

DOI: 10.1021/acs.jpcb.8b06820
J. Phys. Chem. B 2018, 122, 11206−11217

SOFAST/BEST-Type Experiments: Advantages and Limitations. *J. Biomol. NMR* **2014**, *60*, 99−107.
(22) Chevelkov, V.; Xue, Y.; Rao, D. K.; Forman-Kay, J. D.; Skrynnikov, N. R. $^{15}N^{H/D}$-SOLEXSY Experiment for Accurate Measurement of Amide Solvent Exchange Rates: Application to Denatured drkN SH3. *J. Biomol. NMR* **2010**, *46*, 227−244.
(23) Thakur, A.; Chandra, K.; Dubey, A.; D'Silva, P.; Atreya, H. S. Rapid Characterization of Hydrogen Exchange in Proteins. *Angew. Chem., Int. Ed.* **2013**, *52*, 2440−2443.
(24) Kateb, F.; Pelupessy, P.; Bodenhausen, G. Measuring Fast Hydrogen Exchange Rates by NMR Spectroscopy. *J. Magn. Reson.* **2007**, *184*, 108−113.
(25) Segawa, T.; Kateb, F.; Duma, L.; Bodenhausen, G.; Pelupessy, P. Exchange Rate Constants of Invisible Protons in Proteins Determined by NMR Spectroscopy. *ChemBioChem* **2008**, *9*, 537−542.
(26) Forsén, S.; Hoffman, R. A. Study of Moderately Rapid Chemical Exchange Reactions by Means of Nuclear Magnetic Double Resonance. *J. Chem. Phys.* **1963**, *39*, 2892−2901.
(27) Ward, K. M.; Aletras, A. H.; Balaban, R. S. A New Class of Contrast Agents for MRI Based on Proton Chemical Exchange Dependent Saturation Transfer (CEST). *J. Magn. Reson.* **2000**, *143*, 79−87.
(28) van Zijl, P. C. M.; Yadav, N. N. Chemical Exchange Saturation Transfer (CEST): What Is in a Name and What Isn't? *Magn. Reson. Med.* **2011**, *65*, 927−948.
(29) Vallurupalli, P.; Bouvignies, G.; Kay, L. E. Studying "Invisible" Excited Protein States in Slow Exchange with a Major State Conformation. *J. Am. Chem. Soc.* **2012**, *134*, 8148−8161.
(30) Anthis, N. J.; Clore, G. M. Visualizing Transient Dark States by NMR Spectroscopy. *Q. Rev. Biophys.* **2015**, *48*, 35−116.
(31) Yuwen, T.; Kay, L. E.; Bouvignies, G. Dramatic Decrease in CEST Measurement Times Using Multi-Site Excitation. *ChemPhysChem* **2018**, *19*, 1707−1710.
(32) Yuwen, T.; Bouvignies, G.; Kay, L. E. Exploring Methods to Expedite the Recording of CEST Datasets Using Selective Pulse Excitation. *J. Magn. Reson.* **2018**, *292*, 1−7.
(33) Leninger, M.; Marsiglia, W. M.; Jerschow, A.; Traaseth, N. J. Multiple Frequency Saturation Pulses Reduce CEST Acquisition Time for Quantifying Conformational Exchange in Biomolecules. *J. Biomol. NMR* **2018**, *71*, 19−30.
(34) Nott, T. J.; Petsalaki, E.; Farber, P.; Jervis, D.; Fussner, E.; Plochowietz, A.; Craggs, T. D.; Bazett-Jones, D. P.; Pawson, T.; Forman-Kay, J. D.; et al. Phase Transition of a Disordered Nuage Protein Generates Environmentally Responsive Membraneless Organelles. *Mol. Cell* **2015**, *57*, 936−947.
(35) Brady, J. P.; Farber, P. J.; Sekhar, A.; Lin, Y. H.; Huang, R.; Bah, A.; Nott, T. J.; Chan, H. S.; Baldwin, A. J.; Forman-Kay, J. D.; et al. Structural and Hydrodynamic Properties of an Intrinsically Disordered Region of a Germ Cell-Specific Protein on Phase Separation. *Proc. Natl. Acad. Sci. U. S. A.* **2017**, *114*, E8194−E8203.
(36) Bouvignies, G.; Vallurupalli, P.; Kay, L. E. Visualizing Side Chains of Invisible Protein Conformers by Solution NMR. *J. Mol. Biol.* **2014**, *426*, 763−774.
(37) Zaiss, M.; Bachert, P. Exchange-Dependent Relaxation in the Rotating Frame for Slow and Intermediate Exchange − Modeling Off-Resonant Spin-Lock and Chemical Exchange Saturation Transfer. *NMR Biomed.* **2013**, *26*, 507−518.
(38) Guenneugues, M.; Berthault, P.; Desvaux, H. A Method for Determining B_1 Field Inhomogeneity. Are the Biases Assumed in Heteronuclear Relaxation Experiments Usually Underestimated? *J. Magn. Reson.* **1999**, *136*, 118−126.
(39) Geen, H.; Freeman, R. Band-Selective Radiofrequency Pulses. *J. Magn. Reson.* **1991**, *93*, 93−141.
(40) Delaglio, F.; Grzesiek, S.; Vuister, G. W.; Zhu, G.; Pfeifer, J.; Bax, A. NMRPipe: A Multidimensional Spectral Processing System Based on Unix Pipes. *J. Biomol. NMR* **1995**, *6*, 277−293.
(41) GitHub. *ChemEx Repository*; https://github.com/gbouvignies/chemex (accessed August 30, 2018).
(42) Vallurupalli, P.; Sekhar, A.; Yuwen, T.; Kay, L. E. Probing Conformational Dynamics in Biomolecules via Chemical Exchange Saturation Transfer: A Primer. *J. Biomol. NMR* **2017**, *67*, 243−271.
(43) Lopez, J.; Ahuja, P.; Landrieu, I.; Cantrelle, F. X.; Huvent, I.; Lippens, G. H/D Exchange of a ^{15}N Labelled Tau Fragment As Measured by a Simple Relax-EXSY Experiment. *J. Magn. Reson.* **2014**, *249*, 32−37.
(44) Bodenhausen, G.; Freeman, R.; Morris, G. A. A Simple Pulse Sequence for Selective Excitation in Fourier Transform NMR. *J. Magn. Reson.* **1976**, *23*, 171−175.
(45) Morris, G. A.; Freeman, R. Selective Excitation in Fourier-Transform Nuclear Magnetic Resonance. *J. Magn. Reson.* **1978**, *29*, 433−462.
(46) Sekhar, A.; Rumfeldt, J. A. O.; Broom, H. R.; Doyle, C. M.; Bouvignies, G.; Meiering, E. M.; Kay, L. E. Thermal Fluctuations of Immature SOD1 Lead to Separate Folding and Misfolding Pathways. *eLife* **2015**, *4*, No. e07296, DOI: 10.7554/eLife.07296.
(47) Charlier, C.; Bouvignies, G.; Pelupessy, P.; Walrant, A.; Marquant, R.; Kozlov, M.; De Ioannes, P.; Bolik-Coulon, N.; Sagan, S.; Cortes, P.; et al. Structure and Dynamics of an Intrinsically Disordered Protein Region That Partially Folds upon Binding by Chemical-Exchange NMR. *J. Am. Chem. Soc.* **2017**, *139*, 12219−12227.
(48) Sekhar, A.; Velyvis, A.; Zoltsman, G.; Rosenzweig, R.; Bouvignies, G.; Kay, L. E. Conserved Conformational Selection Mechanism of Hsp70 Chaperone−Substrate Interactions. *eLife* **2018**, *7*, No. e32764, DOI: 10.7554/eLife.32764.
(49) Wang, A. C.; Grzesiek, S.; Tschudin, R.; Lodi, P. J.; Bax, A. Sequential Backbone Assignment of Isotopically Enriched Proteins in D_2O by Deuterium-Decoupled HA(CA)N and HA(CACO)N. *J. Biomol. NMR* **1995**, *5*, 376−382.
(50) Abragam, A. *The Principles of Nuclear Magnetism*; Clarendon Press: Oxford, U.K., 1961.
(51) Levitt, M. H. Symmetrical Composite Pulse Sequences for NMR Population Inversion. II. Compensation of Resonance Offset. *J. Magn. Reson.* **1982**, *50*, 95−110.
(52) Shaka, A. J.; Lee, C. J.; Pines, A. Iterative Schemes for Bilinear Operators; Application to Spin Decoupling. *J. Magn. Reson.* **1988**, *77*, 274−293.
(53) Schmidt, J. M.; Hua, Y.; Löhr, F. Correlation of ^2J Couplings with Protein Secondary Structure. *Proteins: Struct., Funct., Bioinf.* **2010**, *78*, 1544−1562.
(54) Bystrov, V. F. Spin−Spin Coupling and the Conformational States of Peptide Systems. *Prog. Nucl. Magn. Reson. Spectrosc.* **1976**, *10*, 41−82.
(55) Bax, A.; Ikura, M.; Kay, L. E.; Torchia, D. A.; Tschudin, R. Comparison of Different Modes of Two-Dimensional Reverse-Correlation NMR for the Study of Proteins. *J. Magn. Reson.* **1990**, *86*, 304−318.
(56) Shaka, A. J.; Keeler, J.; Frenkiel, T.; Freeman, R. An Improved Sequence for Broadband Decoupling: WALTZ-16. *J. Magn. Reson.* **1983**, *52*, 335−338.
(57) Kay, L. E.; Keifer, P.; Saarinen, T. Pure Absorption Gradient Enhanced Heteronuclear Single Quantum Correlation Spectroscopy with Improved Sensitivity. *J. Am. Chem. Soc.* **1992**, *114*, 10663−10665.
(58) Schleucher, J.; Sattler, M.; Griesinger, C. Coherence Selection by Gradients without Signal Attenuation: Application to the Three-Dimensional HNCO Experiment. *Angew. Chem., Int. Ed. Engl.* **1993**, *32*, 1489−1491.
(59) Marion, D.; Ikura, M.; Tschudin, R.; Bax, A. Rapid Recording of 2D NMR-Spectra without Phase Cycling. Application to the Study of Hydrogen Exchange in Proteins. *J. Magn. Reson.* **1989**, *85*, 393−399.
(60) Pelupessy, P.; Chiarparin, E.; Bodenhausen, G. Excitation of Selected Proton Signals in NMR of Isotopically Labeled Macromolecules. *J. Magn. Reson.* **1999**, *138*, 178−181.
(61) Pelupessy, P.; Chiarparin, E. Hartmann−Hahn Polarization Transfer in Liquids: An Ideal Tool for Selective Experiments. *Concepts Magn. Reson.* **2000**, *12*, 103−124.
(62) McConnell, H. M. Reaction Rates by Nuclear Magnetic Resonance. *J. Chem. Phys.* **1958**, *28*, 430−431.

DOI: 10.1021/acs.jpcb.8b06820
J. Phys. Chem. B 2018, 122, 11206−11217

(63) Loh, S. N.; Markley, J. L. In *Techniques in Protein Chemistry*; Angeletti, R. H., Ed.; Academic Press: London, U.K., 1993; Vol. *4*, pp 517−524.
(64) Englander, S. W.; Poulsen, A. Hydrogen−Tritium Exchange of Random Chain Polypeptide. *Biopolymers* **1969**, *7*, 379−393.
(65) LiWang, A. C.; Bax, A. Equilibrium Protium/Deuterium Fractionation of Backbone Amides in U−^{13}C/^{15}N Labeled Human Ubiquitin by Triple Resonance NMR. *J. Am. Chem. Soc.* **1996**, *118*, 12864−12865.
(66) Bai, Y. W.; Milne, J. S.; Mayne, L.; Englander, S. W. Primary Structure Effects on Peptide Group Hydrogen Exchange. *Proteins: Struct., Funct., Genet.* **1993**, *17*, 75−86.
(67) Connelly, G. P.; Bai, Y. W.; Jeng, M. F.; Englander, S. W. Isotope Effects in Peptide Group Hydrogen Exchange. *Proteins: Struct., Funct., Genet.* **1993**, *17*, 87−92.
(68) Fox Chase Cancer Center. *SPHERE: A Server Program for Hydrogen Exchange Rate Estimation*; https://landing.foxchase.org/research/labs/roder/sphere/ (accessed August 30, 2018).
(69) Lipari, G.; Szabo, A. Model-Free Approach to the Interpretation of Nuclear Magnetic Resonance Relaxation in Macromolecules. 1. Theory and Range of Validity. *J. Am. Chem. Soc.* **1982**, *104*, 4546−4559.
(70) Lipari, G.; Szabo, A. Model-Free Approach to the Interpretation of Nuclear Magnetic Resonance Relaxation in Macromolecules. 2. Analysis of Experimental Results. *J. Am. Chem. Soc.* **1982**, *104*, 4559−4570.
(71) Hiyama, Y.; Niu, C. H.; Silverton, J. V.; Bavoso, A.; Torchia, D. A. Determination of ^{15}N Chemical Shift Tensor via ^{15}N−^{2}H Dipolar Coupling in Boc-glycylglycyl[^{15}N]glycine Benzyl Ester. *J. Am. Chem. Soc.* **1988**, *110*, 2378−2383.
(72) Kay, L. E.; Torchia, D. A.; Bax, A. Backbone Dynamics of Proteins As Studied by ^{15}N Inverse Detected Heteronuclear NMR Spectroscopy: Application to Staphylococcal Nuclease. *Biochemistry* **1989**, *28*, 8972−8979.
(73) Xu, J.; Millet, O.; Kay, L. E.; Skrynnikov, N. R. A New Spin Probe of Protein Dynamics: Nitrogen Relaxation in ^{15}N−^{2}H Amide Groups. *J. Am. Chem. Soc.* **2005**, *127*, 3220−3229.
(74) Vasos, P. R.; Hall, J. B.; Kümmerle, R.; Fushman, D. Measurement of ^{15}N Relaxation in Deuterated Amide Groups in Proteins Using Direct Nitrogen Detection. *J. Biomol. NMR* **2006**, *36*, 27−36.
(75) Keiter, E. A. Deuterium and Nitrogen-14 Nuclear Quadrupole Double Resonance Studies of Hydrogen Bonding. Ph.D. Dissertation, University of Illinois at Urbana−Champaign, Champaign, IL, 1986.
(76) Vallurupalli, P.; Kay, L. E. Probing Slow Chemical Exchange at Carbonyl Sites in Proteins by Chemical Exchange Saturation Transfer NMR Spectroscopy. *Angew. Chem., Int. Ed.* **2013**, *52*, 4156−4159.
(77) Korzhnev, D. M.; Religa, T. L.; Banachewicz, W.; Fersht, A. R.; Kay, L. E. A Transient and Low-Populated Protein-Folding Intermediate at Atomic Resolution. *Science* **2010**, *329*, 1312−1316.
(78) Yuwen, T.; Brady, J. P.; Kay, L. E. Probing Conformational Exchange in Weakly Interacting, Slowly Exchanging Protein Systems via Off-Resonance $R_{1\rho}$ Experiments: Application to Studies of Protein Phase Separation. *J. Am. Chem. Soc.* **2018**, *140*, 2115−2126.
(79) Abildgaard, J.; Hansen, P. E.; Manalo, M. N.; LiWang, A. Deuterium Isotope Effects on ^{15}N Backbone Chemical Shifts in Proteins. *J. Biomol. NMR* **2009**, *44*, 119−126.
(80) Perelman School of Medicine, University of Pennsylvania. *Englander Lab Home Page: Download*; http://hx2.med.upenn.edu/download.html (accessed August 30, 2018).

DOI: 10.1021/acs.jpcb.8b06820
J. Phys. Chem. B 2018, 122, 11206−11217